Soil carbon dioxide flux partitioning in a calcareous watershed with agricultural impacts

Caitlin Hodges[1*], Susan L. Brantley[2,3], Melika Sharifironizi[2], Brandon Forsythe[2], Qicheng Tang[1], Nathan Carpenter[3], Jason Kaye[1]

[1]Pennsylvania State University, Department of Ecosystem Science and Management, University Park, PA

[2]Pennsylvania State University, Earth and Environmental Systems Institute, University Park, PA

[3]Pennsylvania State University, Department of Geosciences, University Park, PA

Corresponding author: Caitlin Hodges (cah423@psu.edu)

Key Points:

- Carbonate mineralogy increases the dissolved inorganic carbon flux out of soils in an agricultural, humid temperate watershed
- This flux of dissolved inorganic carbon represents 43% of all respired carbon dioxide in the soil containing the most carbonates
- Surface carbon dioxide efflux measurements would substantially underestimate soil respiration rates in this watershed

Abstract

Predicting the partitioning between aqueous and gaseous C across landscapes is difficult because many factors interact to control CO_2 concentrations and removal as DIC. For example, carbonate minerals may buffer soil pH so that CO_2 dissolves in porewaters, but nitrification of fertilizers may decrease pH so that carbonate weathering results in a gaseous CO_2 efflux. Here, we investigate CO_2 production and dissolution in an agricultural, first-order, mixed-lithology humid, temperate watershed. We quantified soil mineralogy and measured porewater chemistry, soil moisture, and pCO_2 and pO_2 as a function of depth at three hillslope positions for a year. The variation of soil moisture along the hillslope was the dominant control on the concentration of soil CO_2, but mineralogy acted as a secondary control on the partitioning of CO_2 between the gaseous and aqueous phases. The regression slopes of pCO_2 vs. pO_2 in the carbonate-bearing soils indicate a deficit of CO_2 relative to O_2 ($p < 0.05$). Additionally, we found no abiotic gaseous CO_2 efflux from carbonate weathering. We concluded that in the calcareous soils, about a third of respired C dissolves and drains from the soil rather than diffusing out to the atmosphere. To represent the global scope of the reactions we evaluated at our local watershed, we used databases of carbonate minerals and land uses to map types of soil degassing behaviors. Based on our maps, the partitioning of respired soil CO_2 to the aqueous phase may be globally common and should be accounted for in ecosystem C budgets and models.

Plain Language Summary

Carbon dioxide (CO_2) produced by roots and microbes in soil is a key component of the global carbon cycle. Generally, respired CO_2 exits soil as a gas. However, CO_2 also dissolves in soil porewaters during weathering reactions in soils, especially with carbonate minerals. These reactions reduce the amount of CO_2 exiting the soil surface. Conversrely, agricultural production

may create conditions that drive CO_2 in carbonates into the gas phase. These reactions in agricultural soils may increase the amount of CO_2 leaving the soil surface. We investigated when these reactions may be important in decreasing or increasing the amount of CO_2 exiting the soil surface. In soils containing carbonate minerals, we found that respired CO_2 drove weathering of carbonate minerals and thus decreased the amount of CO_2 that exits the soil surface by one third. We found no evidence of agricultural land use generating conditions that drive CO_2 from carbonate minerals into the gas phase. Our results indicate that measurements of soil surface CO_2 flux measurements would underestimate the amount of CO_2 produced by plant roots and microbes. These reactions are common in soils and should be accounted for in global C cycle models.

1 Introduction

Soil respiration represents a key component of the global carbon (C) cycle, as it is the largest flux of C from terrestrial systems over annual timescales (Amundson, 2001). In many cases, the flux of CO_2 from the soil surface equals the CO_2 produced by respiring roots and organisms in soil (Cerling, 1984). Indeed, most ecosystem carbon cycle models, from plot to global scale, simulate soil CO_2 flux as equivalent to soil respiration (Oleson et al., 2010; Shi et al., 2018; Thornton et al., 2002). Soil C flux (soil respiration) is most often simulated as a function of soil temperature and moisture (Brook et al., 1983; Lloyd & Taylor, 1994; Raich & Schlesinger, 1992). However, respired CO_2 has the potential to participate in a range of reactions in the soil system that may lower the measured soil CO_2 flux by over 50% (Chadwick et al., 1994; Hamerlynck et al., 2013; Hodges et al., 2019; Olshansky et al., 2019; Rey, 2015; Sánchez-Cañete et al., 2018). Indeed, researchers with interest in long-term C cycling emphasize sequestration of C as alkalinity in soil pore fluids during weathering over geological time periods

(Brantley et al., 2014). Incorporating these reactions into modern-day ecosystem models could improve C cycle projections.

Reactions of water and minerals with CO_2 in the soil system are not included in our ecosystem models at least partly because the extent and magnitude of each reaction is unclear, especially for soils formed at different landscape positions or with different mineralogy. For example, Olshansky et al. (2019) report that drainage of soil waters through a midslope soil reduced total CO_2 efflux by two thirds due to dissolution of gaseous CO_2 and removal downslope. Similarly, in calcareous soils, increasing soil water content enhances carbonate dissolution and serves to increase partitioning of inorganic carbon to the aqueous phase (Kim et al., 2020; Mikhailova & Post, 2006; Wu et al., 2008). However, abiotic reactions may also be a source of CO_2 with respect to the soil atmosphere. For example, land management associated with agricultural production can lower soil pH so that weathering of carbonate minerals becomes a source of abiotic CO_2 to the soil atmosphere, augmenting soil CO_2 flux (Sanderman, 2012; West & McBride, 2005; Zamanian et al., 2018). The magnitude of this potential abiotic gaseous CO_2 flux is controlled by soil buffering capacity and nitrification rate (Hamilton et al., 2007). Therefore, our goal was to determine the role of landscape position and mineralogy in the production of CO_2 and the subsequent partitioning of that soil CO_2 between the aqueous and gaseous phase in a humid, temperate watershed affected by agricultural land-use. We then apply our findings to refine predictions of where abiotic reactions with respired CO_2 may impact measurements or models of soil respiration.

Our research site, the Susquehanna Shale Hills Critical Zone Observatory (SSHCZO), is particularly well suited to this work because it includes contrasting lithologies of distinct mineralogy and potential agricultural impacts. We hypothesized 1) that differences in soil

93 moisture by hillslope position would act as first-order controls on soil pCO_2 with wet hillslope
94 positions having higher pCO_2 than dryer positions due to well documented impacts of soil
95 moisture on respiration and diffusion (Brook et al., 1983; Hasenmueller et al., 2015). In this case,
96 soil pO_2 and pCO_2 is expected to follow a 1:1 molar relationship with respect to consumption of
97 O_2 and production of CO_2 following the stoichiometry of aerobic respiration corrected for
98 diffusion. However, we expected that this moisture-driven respiration-diffusion pattern could be
99 affected by mineralogy and nitrification. Specifically, we hypothesized 2) that in soils with more
100 carbonates, the carbonates would buffer soil pH so that some respired CO_2 would be partitioned
101 into the aqueous phase and exported in draining water such that the pCO_2 to pO_2 ratio of the soil
102 atmosphere would be lower than predicted. We additionally hypothesized 3) that this dissolved
103 CO_2 in draining soil waters would represent removal of the respired CO_2 from the soil. This
104 would contrast with our results from the nearby Shale Hills watershed where CO_2 dissolution and
105 subsequent mineral weathering had no significant effect on soil CO_2 efflux on annual timescales
106 (Hasenmueller et al., 2015; Hodges et al., 2019; Jin et al., 2014).

107 For agriculturally impacted soils, we hypothesized 4) that nitrate-associated acidity in
108 porewaters accelerates carbonate mineral dissolution and drives abiotic, mineral-derived CO_2
109 into the gaseous phase. This tests the predictions that nitrification-associated acidity drives
110 carbonate-derived CO_2 into the gas phase (Zamanian et al., 2018, 2021), since acidity produced
111 during nitrification favors lower pH values and therefore, gaseous, rather than dissolved, CO_2.

112 If hypotheses 2 and 3 are supported, then measurements of soil CO_2 efflux at our field
113 site likely underestimate soil respiration. If hypothesis 4 is supported, then soil CO_2 efflux at our
114 site likely represents a combination of respiration and abiotically generated CO_2. Either of these

115 results would represent a significant departure from the standard assumption that soil CO_2 efflux
116 equals soil respiration.

117 To test our hypotheses, we monitored soil pCO_2, pO_2, moisture, temperature, and solution
118 chemistry in soils at three hillslope positions over a growing season in a cultivated landscape
119 developed on carbonate- and silicate-containing lithologies. We then linked the differences in
120 patterns of the soil gases and solution chemistry to moisture and mineralogical differences at
121 each hillslope position. Finally, by considering results at the SSHCZO, we used the World
122 Inventory of Soil Emission Potentials and Global Food Security and Support databases to
123 identify the soils and regions where the presence of carbonate minerals impacts soil pCO_2
124 partitioning between gas and aqueous phases, causing CO_2 flux measurements to be poor
125 predictors of soil respiration.

126 **2 Materials and Methods**

127 2.1 Site Description

128 Measurements were focused in the Cole Farm watershed of the SSHCZO. The SSHCZO is in the
129 Ridge and Valley physiographic province of central Pennsylvania, USA, which is characterized
130 by folded and sometimes steeply dipping sedimentary rock. The Cole Farm catchment of the
131 SSHCZO is a small (0.65 km^{-2}) watershed underlain by calcareous shales of the Wills Creek and
132 Bloomsburg-Mifflintown formations containing interbedded shaley limestone, dolomite,
133 sandstone, and siltstone (Fig. 1; see supplement for mineralogy of local lithologies).

134 This site has been in active agricultural production since the early 1800s (Li et al., 2018).
135 Recent work in the watershed indicates limited sediment erosion from European settlement and
136 agricultural production (Silverhart, 2019). The three hillslope positions are not under agricultural
137 management, but the two midslope soils are downslope of fields in active production. Specific

fertilizer application rates to the agricultural fields upslope of the midslopes are unknown for the 2018 growing season, but urea, $(NH_4)_2SO_4$, $(NH_4)_2HPO_4$, and potash were applied to the fields in addition to cow manure.

Within the catchment, four sites were chosen for soil characterization and long-term monitoring on the east midslope, west midslope, ridgetop, and valley floor. Monitoring of the valley floor site was abandoned due to consistent flooding throughout the growing season. The ridgetop site, CFRT, is located within the Bloomsburg-Mifflintown Formation that remains as a small forested ridge above the cultivated fields. Both midslope sites are downhill of the ridge on Wills Creek Formation. CFRT lies at the head of a swale and the two midslope sites are located

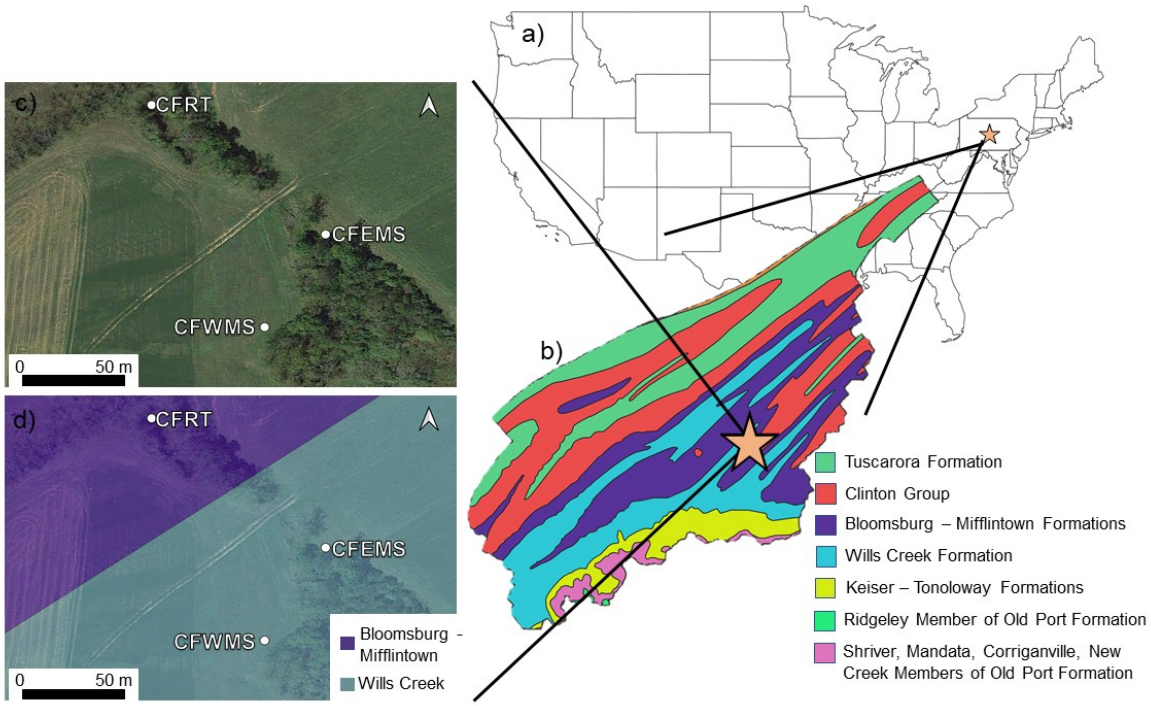

Fig 1: The Cole Farm watershed in the context of the United States (a), the broader Shavers Creek watershed (b), and zoomed-in to indicate vegetation and long-term sampling locations (c), and underlying bedrock formations (d).

along the swale which runs between an eastern and western cultivated field (Fig. 1). The swale collects runoff and groundwater from the surrounding agricultural production.

149

150 2.2 Soil Collection and Geochemical Analysis

151 Soil pits were dug at the east midslope (CFEMS), west midslope (CFWMS), ridgetop (CFRT)
152 locations (Fig. 1). Full soil pit descriptions for each site are published in the supplementary
153 materials of Li et al. (2018). The soils of Cole Farm are characterized by deep, fine particle size
154 class Alfisols. The two midslope soils, developed from calcareous shale of the Wills Creek
155 Formation, show little carbonate mineral content in the upper horizons, and a large increase in
156 carbonates at the C horizon. This is interpreted as evidence for almost complete carbonate
157 mineral dissolution in the upper horizons (see, for example, Figure 2), given that most of the
158 unweathered rock units reported in this Formation contain carbonate minerals (see appendix for
159 geochemical analysis of local bedrock). Furthermore, nearby soils similarly show such carbonate
160 depletion at the surface at a site with many sampling locations and wells (Brantley et al., 2013;
161 Gu et al., 2020). The ridgetop soil profile, developed from the Bloomsburg-Mifflintown
162 Formation, shows no evidence of higher carbonate abundance at depth most likely because the
163 parent lithology is not as calcareous as the Wills Creek.

164 Soils were sampled in 10 cm increments to bedrock (where bedrock was defined as the
165 limit of digging by backhoe). Bulk samples of the 10 cm increments representative of distinct
166 horizons were ground and digested using Li metaborate fusion for total elemental analysis.
167 Elemental analysis was performed on fusion digestates on a Perkin-Elmer Optima 5300,
168 Inductively Coupled Plasma Emission Spectrometer (ICP-AES, PerkinElmer, Waltham, MA,
169 USA). The bulk C-horizon samples were also ground to a fine powder and analyzed using X-Ray
170 diffraction with a Malvern Panalytical Empyrean X-Ray Diffractometer (Malvern Panalytical,
171 Malvern, Worcestershire, UK). Results from XRD were interpreted semi-quantitatively using

JADE software (International Centre for Diffraction Data, Newtown Square, PA, USA). Total carbon of the bulk soils was analyzed on a CHNS-O elemental analyzer (Elemental Analyzer EA 1110, Thermo Fisher Scientific, Waltham, MA, USA).

2.3 Soil Gas Collection and Analysis

Soil gas samplers identical to those described in Hasenmueller et al. (2015) were installed in triplicate at depths of interest at the three hillslope positions chosen to study soil gases. At CFEMS and CFWMS soil pits, the gas samplers were installed at 20 cm and 40 cm depths, and at a depth of 20 cm above the Cr horizon, which came to 108 cm in CFEMS and 190 cm in CFWMS. At CFRT soil gas samplers were installed at 20 cm, 40 cm, 90 cm and 160 cm. All statistical analyses were performed with only the data from the 20 and 40 cm gas wells, as the deep wells were often filled with water at the CFEMS and CFWMS sites. Full pCO_2 and pO_2 datasets are published as corresponding data with this publication in Pangaea.

Soil gas tubes were sampled for pCO_2 and pO_2 (vol/vol %) every 3 wks from April 2018 through November 2018. Air-tight syringes with a one-way lock were used to sample the gas tubes for pCO_2. All gas tubes were purged of 5 mL of gas in the 20 and 40 cm samplers, and 10 mL of gas in all samplers deeper than 40 cm to ensure sampling of soil atmosphere, and not dead air in the sampling tube. Then 5 mL of soil gas was collected with the locking syringe for analysis in the laboratory. Afterward, 10 mL of soil gas was sampled for pO_2 using a handheld soil gas analyzer (model 901, Quantek Instruments). The Quantek 901 has a range of 0 to 100% O_2 and an accuracy of ± 0.1 O_2. The Quantek was calibrated using O_2-free gas and ambient air. Three samples of ambient air were collected with locking syringes 30 cm above the ground surface per hillslope position for ambient CO_2. Soil gas samples were analyzed in the laboratory

194 on a flow-through infrared gas analyzer (LI-7000, LiCOR Inc.) within two days of collection.
195 Measurement accuracy is within 1% of measured value.

196 Soil pCO_2 and pO_2 samples were assessed based on the principles of apparent respiratory
197 quotient (ARQ) detailed in Angert et al. (2015) and are presented in this paper as outlined by
198 Hodges et al. (2019). Briefly, the soil gas data are plotted as pCO_2 vs. pO_2, relative to a line
199 defined by a slope of -0.76 and an x-axis origin of 20.95% (the concentration of O_2 in the
200 atmosphere). The line thus represents the 1:1 stoichiometry of the reaction describing oxidation
201 of generic organic matter (CH_2O) by O_2 and CO_2 production during cellular respiration (Eq. 1)
202 corrected for the ratio of the diffusion coefficients of CO_2 and O_2 in air (0.76).

203 $$CH_2O + O_2 \rightarrow H_2O + CO_2 \quad (1)$$

204 Thus, if aerobic respiration and diffusion are the main controls on CO_2 and O_2
205 concentrations in soil then field data should plot relatively tightly near this theoretical line. In
206 contrast, significant deviations from this slope indicate that processes other than aerobic
207 respiration and gas diffusion control the soil pCO_2 or pO_2. The slope of the regression line is then
208 considered to show the predominant reaction defining the ARQ by dividing it by -0.76. An ARQ
209 of ~ 1 represents aerobic respiration (and gas diffusion). Anything above 1 indicates additional
210 CO_2 in the soil atmosphere compared to O_2, predicted based on the stoichiometry of aerobic
211 respiration. An ARQ below 1 indicates either less CO_2 relative to O_2, or less O_2 relative to CO_2
212 than predicted by the reaction stoichiometry (Angert et al., 2015).

213

214 2.4 Soil Porewater Collection and Analysis

215 Two porous cup tension lysimeters (Soil water samplers, 1900 and 1920 series, Soilmoisture
216 Equipment Corp., Santa Barbara, CA, USA) were installed at CFEMS, CFWMS, and CFRT in

June of 2017. The lysimeters were installed in hand-augered holes at 20 cm and the depth of auger refusal - 108 cm at CFEMS, 190 at CFWMS, and 90 cm at CFRT. For each lysimeter, the final auger bucket of the soil was retained, sieved to remove all coarse fragments greater than 2 mm in size, and mixed with DI water to create a slurry. That slurry was poured back into the hole, after which the lysimeter was pushed in so that the slurry completely covered the porous cup. The remaining fill material was sieved to remove coarse fragments greater than 2 mm, and then tamped down around the lysimeter body to refill the hole in the order the soil was removed from the ground.

Soil porewaters were collected at -50 kPa every three weeks from each lysimeter. Samples were filtered with a 0.45-micron filter, an aliquot was acidified and stored in refrigeration prior to analysis and another half was frozen. Acidified porewaters were analyzed for geogenic cations on an ICP-OES (ThermoFisher ICAP 7400 ICP-OES, Thermo Fisher Scientific, Waltham, MA, USA). Un-acidified porewaters were analyzed for Cl^-, Br^-, Fl^-, and SO_4^- on a Dionex 2100 Ion Chromatography System and were analyzed for NO_3^- N and NH_4^+ N using the Vn^{III} method (Doane and Horwath, 2003; Sims et al., 1995).

Porewaters accumulated in lysimeters for up to 24 hours. During that time, we assumed they re-equilibrated with the atmosphere, degassing CO_2. Therefore, we used an equilibrium calculation to determine DIC for the porewaters (Geochemist's Workbench® 12). To complete the calculations, we assumed the alkalinity equaled the sum of the equivalents of strong base cations minus the similar sum for strong acid anions and that the alkalinity and measured pCO_2 together determined the pH of the porewaters as calculated by GWB.

Additionally, The Geochemist's Workbench® 12 was used to calculate the chemical equilibrium state for select soil porewaters using the porewater chemistry data and the measured

soil gas values – pCO_2 and pO_2. The equilibria at different depths at the three hillslope positions over the sampling period were calculated to determine the porewater's saturation state with respect to calcite. The equilibrium distribution of aqueous species and the saturation index of various minerals, including calcite, were determined for each chemical system with enough available chemical constraints, i.e., porewater cation and anion concentrations and pCO_2 and pO_2 values.

We also tracked soil moisture over the 2018 growing season using Stevens Hydra Probe II soil moisture sensors (Stevens Water Monitoring Systems, Portland, OR, USA), installed at 10, 20, 40, and 90 cm below land surface in each soil pit. Measurements were recorded at 10-minute intervals by Campbell Scientific CR1000 dataloggers (Campbell Scientific, Logan, UT, USA) and transmitted via cellular telemetry.

2.5 Calculation of Carbonate Weathering due to Nitrification

To estimate the carbonate weathering from nitrification-associated acidity, we used a charge balance approach (Perrin et al., 2008). We assumed that all Ca^{+2} and Mg^{+2} entered solution via carbonate mineral weathering and all NO_3^- through nitrification of fertilizers and manure. This allowed us to partition carbonate mineral weathering by the proportion of charge from Ca^{+2} + Mg^{+2} balanced by (HCO_3^- + NO_3^-) versus the remaining proportion balanced by HCO_3^- alone. Concentration of these solutes in precipitation is at least one order of magnitude lower than soil porewater concentrations (see supplementary table 3 for monthly averages from 2018 precipitation recorded at a nearby National Atmospheric Deposition Program site). At Cole Farm, most N fertilization is achieved through the application of dairy manures. The organic N in this manure is first converted to amines and urea (Eq. 2). The amines and urea are then

mineralized to produce NH_4^+ (Eqs. 3, 4, 5). Here, R is any complex organic molecule and R-$CH(NH_2)COOH$ refers to the N-containing component of the manure.

$$3\ R\text{-}CH(NH_2)COOH \rightarrow 2\ R\text{-}NH_2 + 2\ CO(NH_2)_2 + CO_2 \quad (2)$$

$$R\text{-}NH_2 + H_2O \rightarrow NH_3 + R\text{-}OH \quad (3)$$

$$CO(NH)_2 + H_2O \rightarrow 2NH_3 + CO_2 \quad (4)$$

$$NH_3 + H_2O \rightarrow NH_4^+ + OH^- \quad (5)$$

The ultimate products of this mineralization (NH_4^+) are oxidized to NO_3^- by chemo-lithoautotrophs (Eq. 6).

$$NH_4^+ + 2\ O_2 \rightarrow NO_3^- + H_2O + 2\ H^+ \quad (6)$$

Summation and simplification of the hydrolysis of ammonia (Eq. 5) and nitrification of ammonium (Eq. 6) results in Equation 7.

$$NH_3 + 2\ O_2 \rightarrow NO_3^- + H_2O + H^+ \quad (7)$$

The nitric acid resulting from this reaction can drive down pH of the soil porewater and/or drive dissolution of minerals. The fastest dissolving minerals in sedimentary rocks such as those at Cole Farm are carbonates. Carbonate minerals (e.g., calcite, dolomite) readily dissolve in the presence of nitric acid (Eq. 8) in parallel to dissolution driven by carbonic acid (Eq. 9).

$$Ca_xMg_{1-x}CO_3 + HNO_3 \rightarrow x\ Ca^{2+} + (1-x)\ Mg^{2+} + HCO_3^- + NO_3^- \quad (8)$$

$$Ca_xMg_{1-x}CO_3 + CO_2 + H_2O \rightarrow x\ Ca^{2+} + (1-x)\ Mg^{2+} + 2\ HCO_3^- \quad (9)$$

At Cole Farm the land managers also apply inorganic $(NH_4)_2SO_4$ to augment the applied manure. Again, the production of protons through nitrification of this fertilizer (Eq. 10) can result in low pH in soils, which can drive the bicarbonate produced in equation 8 to protonate and then ultimately degas if solubility of aqueous CO_2 is superceded. This happens when localized pH is less than about 6 (Stumm & Morgan, 1996; Eq. 11). Equation 12 is a summed

combination of equations 6, 8, and 11 that emphasizes that the reactions can act as a source of abiotic CO_2 to soil flux.

$$(NH_4)_2SO_4 + 2\ O_2 \rightarrow 2\ NO_3^- + SO_4^{-2} + 4\ H^+ + H_2O \quad (10)$$

$$HCO_3^- + H^+ \rightarrow H_2O + CO_2\ (g) \quad (11)$$

$$NH_4^+ + 2\ O_2 + Ca_xMg_{1-x}CO_3 \rightarrow NO_3^- + xCa^{2+} + (1-x)Mg^{2+}\ \ 2\ H_2O + CO_2\ (g) \quad (12)$$

To calculate a rough estimate of the rate of dissolution of carbonate minerals by nitric acid, we estimated the nitric-generated carbonate weathering per month based on the concentration of nitrate in soil porewater, and the rate of porewater lost to groundwater for each month (Eq. 13).

$$\sum_{m}^{\square} ¿¿ \quad (13)$$

Here, m is the indicator for the month, $[x]_m$ is the soil porewater concentration of ion x (here, $NO_3^{-¿¿}$) for month m (mol L^{-1}), P is cumulative precipitation for month m measured at Cole Farm (m $month^{-1}$), I is the average fraction of precipitation that infiltrates to groundwater, here estimated as 0.5 (Li et al., 2017), and 10^3 is a factor to convert L to m^3. This calculation results in CC_N, which is the annual carbonate weathering rate attributed to nitric acid (mol m^{-2} yr^{-1}). This calculation is based on the assumptions of a soil profile experiencing no lateral transfer of solutes, all NO_3^- in solution balanced by Ca^{+2} or Mg^{+2}, and these cations entered solution through the weathering of carbonate minerals such that 1 mole of NO_3^- in solution has resulted in the dissolution of 1 mole of carbonate mineral (Eq. 8). However, there would be no impact on our estimates in the case of lateral transport of nitric acid and subsequent reaction with carbonate minerals in the pedon. Provenance of the acidity produced through nitrification is not important, as we are calculating the reaction of that acidity with the bedrock carbonates. However, if nitric acid reacted with carbonate minerals (or agricultural lime) upslope such that laterally flowing

porewaters containing Ca^{+2} and Mg^{+2} balanced by NO_3^- and HCO_3^- enter the subsurface of CFEMS or CFWMS, our calculation would overestimate carbonate weathering due to nitrification associated acidity.

This calculation is also based on the assumption that all NO_3^- in porewaters is derived from nitrification and that the concentration of NO_3^- in porewaters on one day of the month is representative of the concentration throughout the month. If porewater data were missing for a month, values were interpolated between measured values.

2.6 Calculation of Carbonate Weathering by Carbonic Acid from Respired CO_2

We assumed that the remaining Ca and Mg in solution not balanced by $HCO_3^- + NO_3^-$ from reaction of nitric acid with carbonate minerals and SO_4^{-2} from $(NH_4)_2SO_4$ fertilization is charge balanced by HCO_3^- generated through carbonate weathering reactions (Eq. 9). While a small amount of Ca- and Mg-containing silicate minerals are found in the bedrock, the most reactive minerals by far are carbonates. The concentration of SO_4^{-2} in rainwater is at least an order of magnitude lower than porewater concentrations (Supplementary Table 3) and S concentrations in these soils is low such that pyrite oxidation is an unlikely source of acidity (Table 1). Therefore, for CO_2-driven dissolution of carbonates (Eq. 9), every mole of Ca + Mg in solution is balanced by one HCO_3^- anion derived from CO_2 in the soil atmosphere and one derived from the mineral. This is a reasonable assumption because Ca and Mg make up over 95% of the positive charge in the porewaters, and NO_3^- and DIC make up over 95% of the negative charge. All HCO_3^-, including that derived from the respired CO_2, exits the soil system as DIC rather than diffusing from the soil surface as CO_2 gas, unless there is a significant shift in pH or temperature to cause supersaturation. Thus, a downslope flux of DIC represents a sink for locally respired CO_2 and a potential mechanism that could result in an ARQ < 1 in a particular pedon.

Based on the reaction stoichiometry of carbonate weathering, alkalinity of the deepest lysimeter's porewaters at each hillslope position, and precipitation corrected for evapotranspiration, we estimated the flux of respired CO_2 to the DIC pool at the three hillslope positions (Eq. 14).

$$\sum_{m}^{\square} ¿¿ \quad (14)$$

Here CC_c is the carbonate weathering rate due to carbonic acid. Where porewater data were missing for a month, they were interpolated. Monthly values were summed to estimate the flux over the year.

2.7 Global Carbonate Stock Mapping

We sought to determine the distribution of soils across the globe that were likely to have 1) a significant flux of respired CO_2 as DIC and 2) a significant gaseous flux of abiotic CO_2 to the atmosphere due to carbonate weathering from nitrification associated acidity under low-pH conditions. We mapped soil inorganic carbon stocks using the % mass of $CaCO_3$ in subsurface soil (30 – 100 cm depths) from the World Inventory of Soil Emission Potentials (WISE30sec) world soil database (Batjes, 2016). This database, which bins soil depths as surface (0 – 30 cm) vs. subsurface (30 – 100 cm), estimates the $CaCO_3$ of the two soil depth intervals on the basis of a 0.5 degree grid.

We then classified soils containing carbonates by binned subsurface (30 – 100 cm) soil pH measured in an H_2O slurry, also from the WISE30sec database. We further parsed this classification of soils as irrigated cropland, rainfed cropland, or non-cropland based on the 1 km global grid from the Global Food Security Support Analysis Data (Thenkabail et al., 2016). We used these datasets to classify carbonate-bearing soils into two types of soil as follows:

1) In neutral and basic soils, CO_2 is likely to dissolve because pH > 5.5. In these soils, respired CO_2 may therefore be removed commonly from the soil atmosphere by dissolution into porewater to form DIC, followed by porewater drainage. In this case, the CO_2 flux out of the soil at the land surface is lower than the actual in situ soil respiration. For these soils, in situ respiration rates are likely higher than measured gaseous CO_2 flux from the soil, confounding ecosystem C budgets.

2) In acidifying soils (pH < 5.5) under agricultural land use that also contain carbonates in the subsurface, nitrification of fertilizers and manures applied to these agricultural lands are likely to dissolve carbonates while maintaining low pH in soil porewaters. This low pH favors release of abiotic, carbonate-derived CO_2 into the gas phase. This abiotic source could increase the surface soil CO_2 efflux (Zamanian et al., 2018, 2021) above that of soil respiration rates. For these soils, measured CO_2 flux from the soil is higher than in situ respiration, again, confounding ecosystem C budgets.

All mapping and raster analyses were performed in ArcMap (ArcMap Desktop Pro version 10.7, ESRI, Redlands, CA).

2.8 Statistical Analysis

Statistical analyses were performed using R (R Core Team, 2019) software. Interpolation maps were generated using the krig function in the fields package for R (Nychka et al., 2015). This function was used to plot hand sampled gas measurements with depth over time. All interpolations were created with the same parameters; l = 1, q = 50, covariance structure = Mattern. Soil surface boundary conditions were set at 0.04% for the CO_2 interpolation, and 20.95% for the O_2 interpolation.

Lines of best fit for plots of pCO_2 versus pO_2 at each hillslope position were generated using the linear modeling (lm) function in R. Regression slopes at each hillslope position were tested for significant differences using the analysis of variance (aov) function in R. Slopes were determined to be significantly different if interactions between the independent variable (site position) with the covariate, pO_2, were significant. Repeated measures ANOVA were used to assess changes in pCO_2 and pO_2 over the growing season.

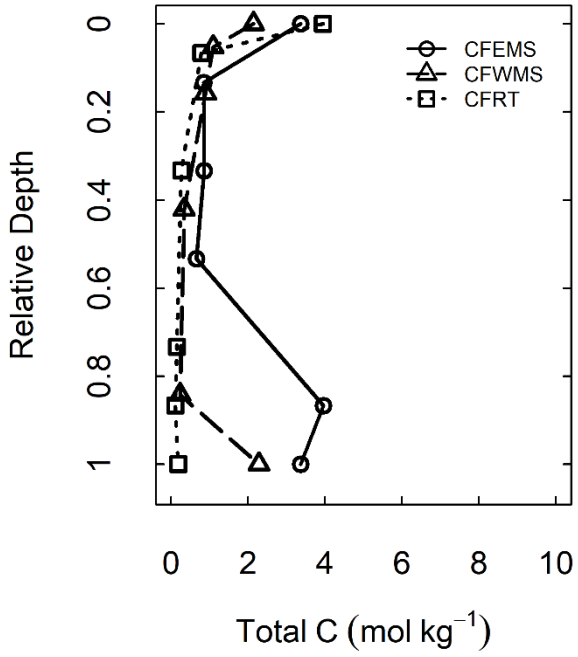

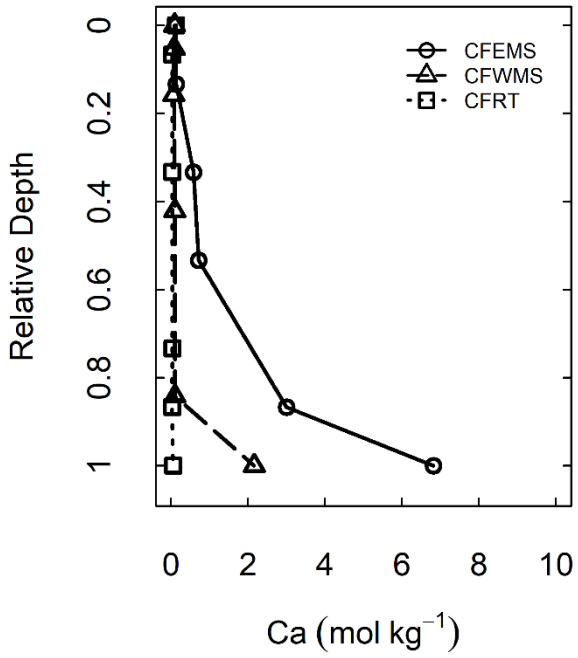

e
east midslope (CFEMS), west midslope (CFWMS), and
are
between
ions.

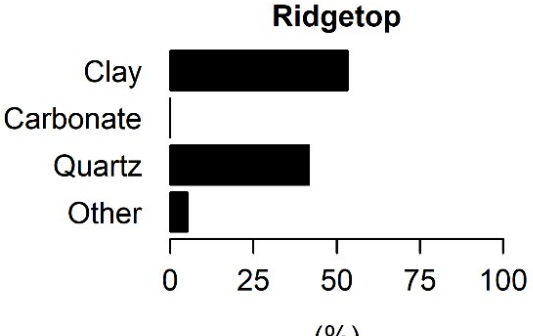

3 Results

3.1 Soil Elemental Analysis

Total elemental analysis by soil horizon and mineral composition of the C horizons of each hillslope position indicate soils of different elemental composition (Table 1, Fig. 2). Our results indicate that CFEMS is dominated by carbonate minerals in the soil subsurface. CFWMS consists of a mix of silicates and carbonates in the subsurface, and CFRT contains no carbonate minerals.

The most striking difference in base cation concentrations among the three soils

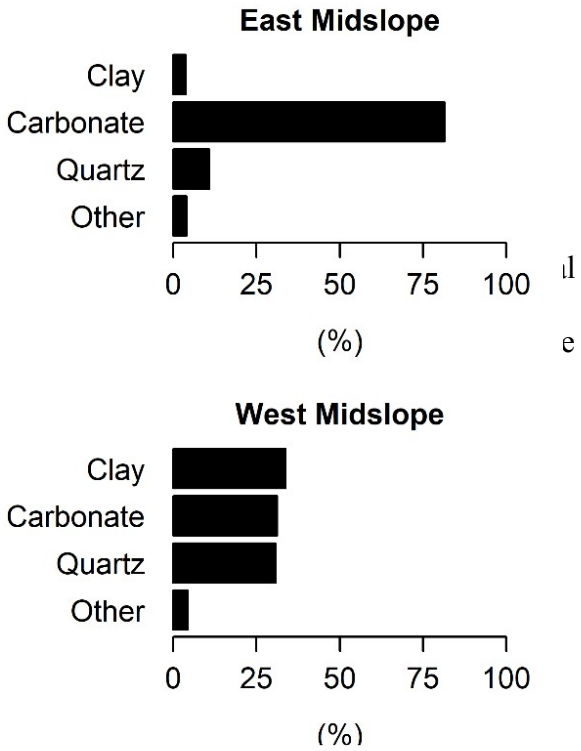

Fig 3: Distribution of minerals in the C horizons of the east midslope (CFEMS), west midslope (CFWMS), and ridgetop (CFRT) soils at Cole Farm.

398 is the Ca concentrations (Fig. 2, Table 1). The
399 markedly from CFEMS to CFWMS to CFRT,
400 content inferred from XRD (Figure 3). Depth
401 CFWMS soils increase from 0.34 wt. % to 8.6
402 horizon sample at 190 cm. The largest increas
403 soil profile at CFEMS between the BC and th
404 concentrations than the WMS soils at all dept
405 to 27.3% from the soil surface to the C horizo
406 soils, the ridgetop does not have high Ca conc
407 than increase with depth, Ca decreases from 0
408 profile. Total C concentrations (Fig. 2) are consistent with the interpretation that these base
409 cation concentrations at CFWMS and CFEMS are indicative of the concentrations of carbonate
410 minerals. Total C concentration is high at the surface of all soil profiles, then it decreases below
411 the surface sample before increasing again in the subsurface of CFWMS and CFEMS, but not
412 CFRT. The mineral composition of the profiles confirms that the C at depth is associated with
413 carbonate minerals (Fig. 3). Based on the XRD data, about 85% of the C horizon by mass at
414 CFEMS consists of carbonate minerals. At CFWMS there is an equal mix of carbonates, layer
415 silicates, and quartz, with each accounting for about 30% of the minerals present in the C
416 horizon. At the ridgetop, carbonates were negligible and quartz and layer silicates comprise
417 about 85% of the minerals (Fig. 3).

418 3.2 Soil Moisture

419 Soil moisture differed at the three
420 hillslope positions (Fig. 4). In

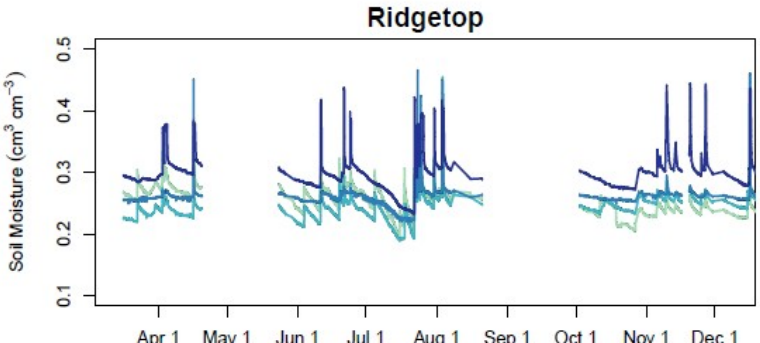

421 general, the two midslope soils, CFEM
422 conditions than CFRT. Assuming the m
423 depth represents saturated conditions, t
424 subsurface (40 – 90 cm) through much
425 contrast, the CFRT soils did not mainta
426 (Fig. 4).

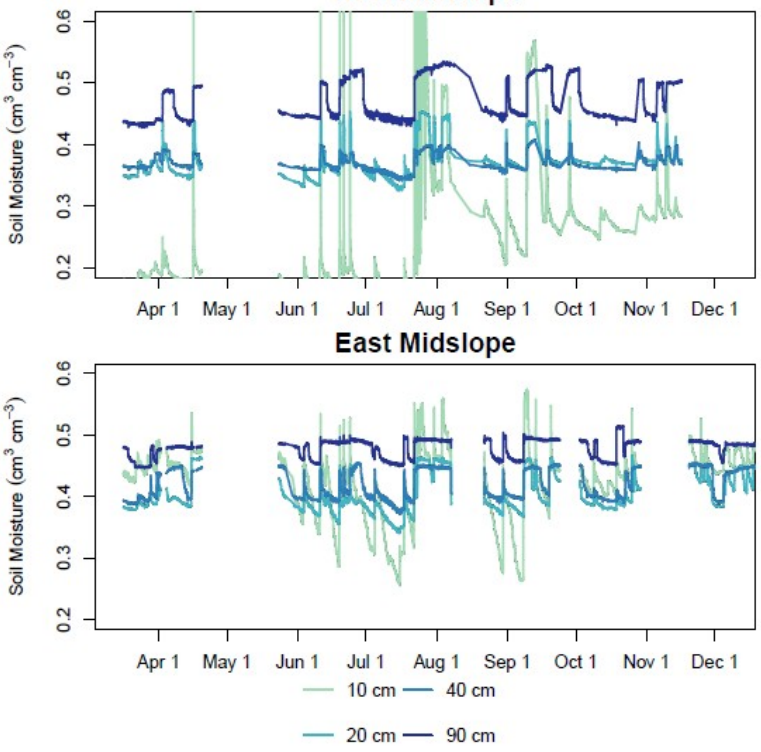

(CFRT), East Midslope (CFEMS), and West Midslope (CFWMS) at Cole Farm. Values are reported as volumetric water content.

Table 1: Elemental concentrations of soils (wt. % unless otherwise noted). Major element oxides and LOI sum to 100 ± 2%

Site	Horizon	Depth (cm)	Al	Ca	Fe	K	Mg	Mn	Na	P	Si	Ti	LOI (900C)	S	Zr (ppm)	Sr (ppm)
West Midslope	Ap	0-10	5.12	0.34	4.29	2.61	0.77	0.15	0.26	0.11	29.6	0.61	10.3	0.03	270	bd*
West Midslope	Bt1	20-30	5.24	0.29	4.33	2.58	0.75	0.18	0.25	0.07	30.8	0.64	7.56	0.02	290	bd*
West Midslope	Bt2	30-40	4.75	0.27	3.93	2.20	0.63	0.19	0.30	0.07	32.4	0.67	6.88	0.01	310	bd*
West Midslope	Bt3	80-90	6.00	0.37	4.67	2.61	0.92	0.09	0.42	0.04	30.1	0.53	7.52	0.00	280	bd*
West Midslope	BC	160-170	6.28	0.39	5.33	3.24	1.16	0.12	0.30	0.07	29.3	0.52	6.61	0.01	290	bd*
West Midslope	C	190-200	6.32	8.65	4.31	3.61	1.25	0.06	0.19	0.05	21.4	0.45	14.4	0.01	160	170
East Midslope	Ap	0-10	5.36	0.52	4.35	2.91	0.89	0.09	0.17	0.10	28.1	0.56	13.6	0.05	250	bd*
East Midslope	Bt1	20-30	5.44	0.53	4.57	2.81	0.86	0.11	0.18	0.06	30.8	0.62	7.11	0.01	270	bd*
East Midslope	Btx	50-60	7.21	2.32	6.05	4.00	1.42	0.12	0.14	0.09	24.9	0.46	9.47	0.01	190	bd*
East Midslope	BC	80-90	7.94	2.87	3.39	5.02	1.30	0.04	0.18	0.07	25.9	0.55	7.51	0.01	190	bd*
East Midslope	C	130-140	4.23	12.0	5.68	2.20	2.78	0.17	0.10	0.07	16.5	0.29	20.8	0.01	170	250
East Midslope	C	150-160	1.43	27.3	3.85	0.78	2.01	0.15	0.06	0.06	6.50	0.11	34.2	0.01	78	760
Ridgetop	A	0-10	4.59	0.51	3.85	2.19	0.58	0.19	0.19	0.14	27.7	0.61	17.3	0.05	320	bd*
Ridgetop	AB	10-20	4.99	0.11	5.39	2.42	0.75	0.18	0.24	0.10	31.8	0.63	5.75	0.01	360	bd*
Ridgetop	Bt1	50-60	5.36	0.11	4.97	2.79	0.71	0.10	0.24	0.07	32.7	0.64	4.36	0.00	390	bd*
Ridgetop	Bt2	110-120	6.00	0.12	4.37	3.58	0.78	0.01	0.24	0.06	31.8	0.62	3.86	0.00	240	bd*
Ridgetop	C	130-140	8.18	0.10	4.88	5.2	1.07	0.0	0.14	0.03	27.5	0.6	4.58	0.00	190	bd*

Ridgetop	Cr	150-160	6.77	0.19	5.67	3 4.3 3	0.96	1 0.0 1	0.15	0.08	29.3	0 0.6 1	4.13	0.00	440	bd*

*Below detection limit

427

3.3 Soil pCO_2 and pO_2

Soil pCO_2 at the three hillslope positions followed the same seasonal and depth trends but differed in concentration by hillslope position when controlling for sampling date and accounting for sampling depth (Fig. 5; $p < 0.001$). In the top 40 cm, we measured the highest pCO_2 in CFEMS, followed by CFWMS. CFRT showed a pCO_2 consistently lower than the two other hillslope positions. All three sites increased from a low concentration of pCO_2 around atmospheric levels at the beginning of the growing season in May to about 3% CO_2 at 40 cm depths in mid-August. However, the CFEMS soils reached higher pCO_2 earlier in the growing season than the CFWMS and CFRT soils (Fig. 5).

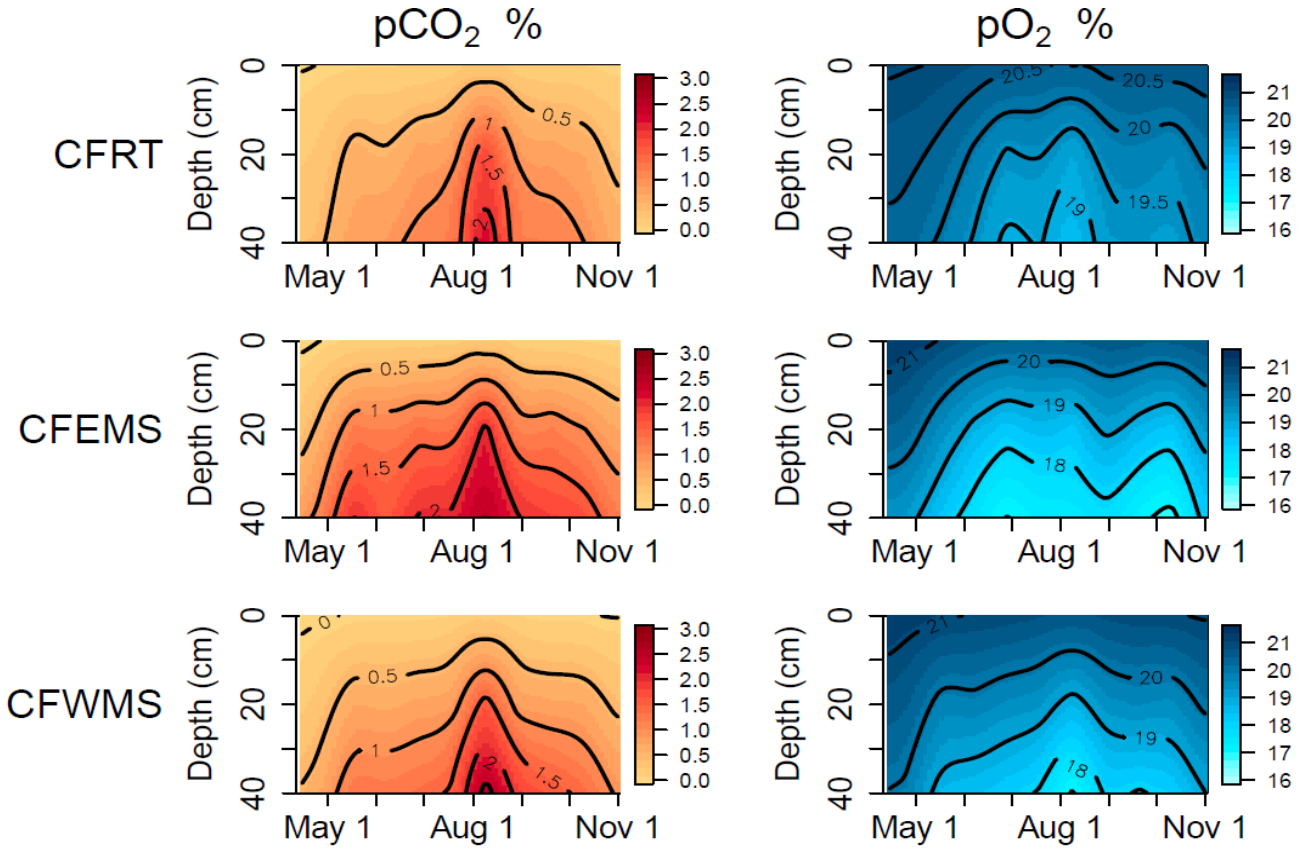

Fig 5. Interpolated graphs of soil pCO_2 (%) and pO_2 (%) as a function of depth over the 2018 growing season in the top 40 cm of the east midslope (CFEMS), west midslope (CFWMS), and ridgetop (CFRT) soils. Darker orange indicates higher pCO_2. Lighter blue represents lower pO_2.

437 Soil pO_2 also differed by hillslope position when controlling for sampling date and depth
438 (Fig. 5, $p = 0.004$). The CFEMS and CFWMS pO_2 was lower than that of CFRT. All three soils
439 experienced lowest pO_2 in August. While CFRT reached a low around 17%, CFEMS and
440 CFWMS reached a low around 16%. At all hillslope positions soil pO_2 decreased from around
441 atmospheric concentrations in April to a low in August and September. The low pO_2 in the soil
442 subsurface lasted longer than the high of pCO_2 (Fig. 5)

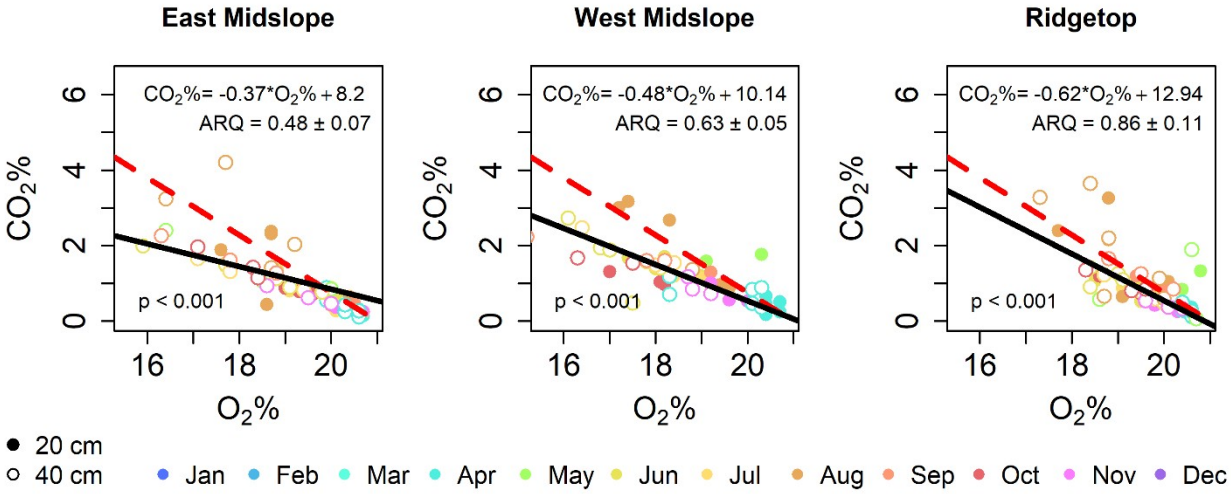

Fig 6: Plots of pO_2 vs. pCO_2 from 20 and 40 cm gas wells in the Cole Farm soils during the 2018 growing season. The dashed line represents the theoretical relationship between pO_2 and pCO_2 governed by aerobic respiration and diffusion (ARQ=1). The solid black line and the equation at the bottom of each plot represents the regression line of best fit through the gas data. Open circles represent samples collected from 40 cm and closed circles are samples collected from 20 cm.

443 Regressions of soil pCO_2 vs. pO_2 differ by hillslope position (Fig. 6). The ANCOVA of
444 soil pCO_2 vs. pO_2 by hillslope position (for 20 cm and 40 cm depths), yields regression slopes for
445 CFEMS (-0.37 ± 0.05) and CFWMS (-0.48 ± 0.04) soils that differ significantly ($p < 0.01$) from
446 the CFRT soil (-0.65 ± 0.08). Likewise, the CFEMS and CFWMS regressions are significantly
447 different from the slope of -0.76 that is consistent with aerobic respiration (+diffusion). The
448 dominant ARQs consistent with the slopes for CFEMS, CFWMS, and CFRT are 0.48 ± 0.07,

449 0.63 ± 0.05, and 0.86 ± 0.11, respectively. The regression slopes and ARQs for CFEMS and
450 CFWMS are consistent with processes that lower the concentration of CO_2 in the gas phase
451 compared to O_2 in comparison to the ratios expected based on aerobic respiration (Hodges et al.,
452 2019).

453 3.4 Soil Porewater Chemistry

454 Concentrations of geogenic cations in porewater solutions varied by hillslope position and time
455 over the 2018 growing season (Fig. 7). In general, the solute concentrations in CFEMS and
456 CFWMS porewaters were higher than the CFRT porewaters; for example, [Ca] and [Mg] were
457 higher in the near-swale soils than the ridge soils. Additionally, [Ca] and [Mg] increased over the
458 growing season but were generally higher in the deep lysimeters than in the shallow lysimeters
459 year-round. On the other hand, Si concentrations did not vary by hillslope position and were
460 higher in the surface than subsurface. The concentrations of Na and K in general were also
461 higher in CFWMS and CFEMS than CFRT throughout the growing season.

462 Anion concentrations in the lysimeters also varied by hillslope position throughout the
463 2018 growing season (Fig. 7). In general, all anions were higher in concentration in the
464 subsurface of CFWMS and CFEMS than at the surface or at any depth at CFRT. In the
465 subsurface of CFWMS, NO_3^- - N was around 4 ppm and was consistently highest throughout the
466 growing season, followed by CFEMS which increased from around 1.5 ppm to 4.5 ppm in
467 August. On the other hand, CFRT NO_3^- - N was consistently lower than the other two sites,
468 around 1 ppm throughout the growing season. Surface concentrations of NO_3^- - N were in
469 general lower than in the subsurface, except at CFEMS in July and August.

470 Alkalinity, pH, and calcite saturation index calculated with GWB varied by pedon (Table
471 2) following the differences in measured porewater anions and cations and mineralogy.

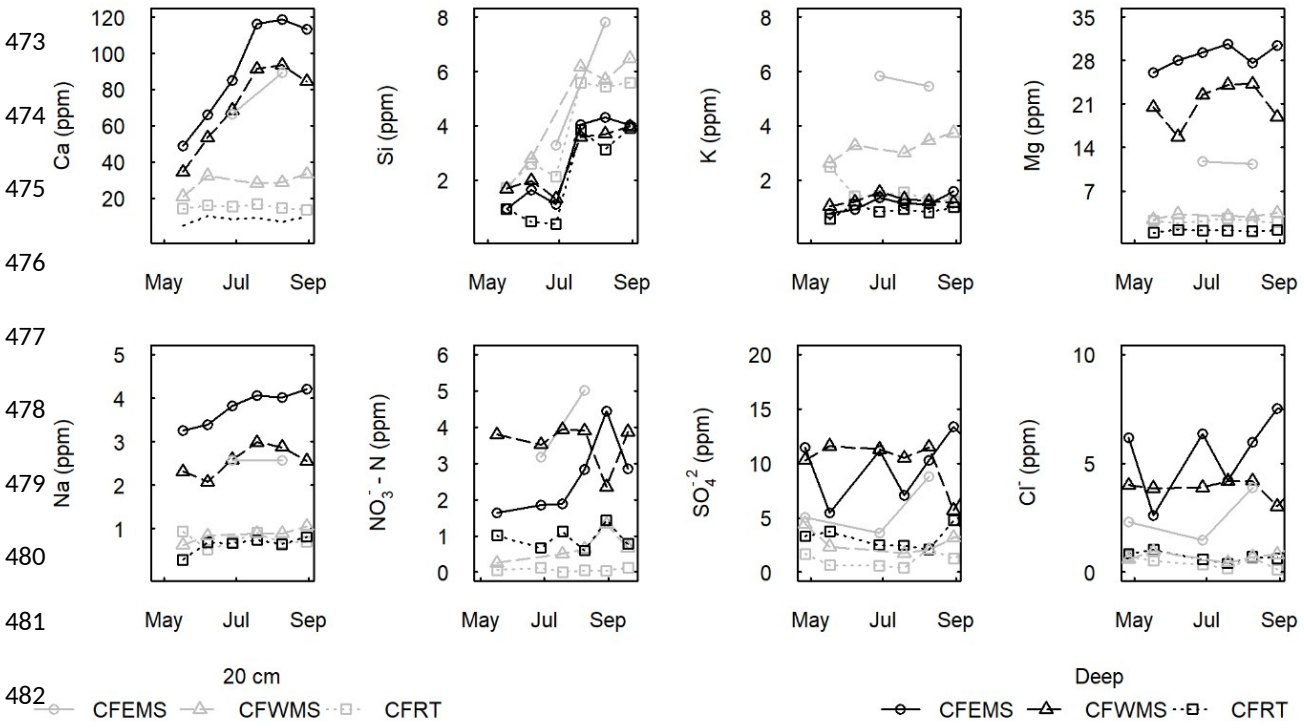

Fig 7: Major solute concentrations in soil water collected from lysimeters at east midslope (CFEMS), west midslope (CFWMS), and ridgetop (CFRT) soils over the 2018 growing season. Gray represents 20 cm lysimeters and black represents subsurface lysimeters at 108, 190, and 90 cm at CFEMS, CFWMS, and CFRT, respectively.

(CFEMS)			8/9/2018	4.76	6.98	0.06 oversat
	108	X	5/17/2018	4.41	7.18	-0.02 eq
		X	7/19/2018	8.05	7.19	0.57 oversat
West Midslope	20		5/17/2018	1.23	7.04	-0.98
(CFWMS)			7/19/2018	1.67	7.11	-0.66
			8/9/2018	1.68	6.65	-1.11
			8/30/2018	1.89	7.47	-0.20
Ridgetop	20		6/28/2018	0.81	6.68	-1.64
(CFRT)			7/19/2018	0.96	6.94	-1.28
			8/9/2018	0.81	6.38	-1.97
			8/30/2018	0.76	6.92	-1.48
	90		6/28/2018	0.41	6.32	-2.53
			7/19/2018	0.42	6.48	-2.34
			8/9/2018	0.33	5.86	-3.17
			8/30/2018	0.39	6.28	-2.54

484 3.5 Estimates of Carbonate Weathering due to Nitrification and Carbonic Acid
485 At CFEMS, CC_N was estimated at the rate of about 0.27 mol carbonate m^{-2} yr^{-1}. Accounting for
486 $CC_N + CC_c$ (i.e. total carbonate dissolution), weathering due to nitrification associated acidity
487 accounts for 5.4% of all carbonate dissolution at the CFEMS position. At CFWMS, because
488 there is a higher concentration of NO_3^- over much of the growing season and a lower
489 concentration of Ca and Mg (consistent with the lower carbonate mineral abundance), CC_N was
490 estimated at about 0.39 mol m^{-2} yr^{-1} and this accounts for 11% of all carbonate weathering. The
491 calculated pH of the porewaters at the midslopes is higher than 6 (Table 2). Our calculations
492 indicate that NO_3^- in the carbonate-derived soils promotes carbonate dissolution but not a
493 gaseous CO_2 flux, because of the high pH that is maintained. Therefore, while weathering of
494 carbonate minerals by nitric acid may on occasion drive CO_2 into the gaseous phase in
495 microsites, the generally higher pCO_2 and buffering capacity of the carbonate rocks favors
496 dissolution of CO_2 in porewaters and loss of C from the soil as HCO_3^- (Gandois et al., 2011).
497 Therefore, we estimate that there is no abiotic gaseous CO_2 flux from the reaction of carbonate
498 minerals with acidity produced through nitrification in any of the Cole Farm soils.
499 We also calculated the rate of reaction of carbonate minerals in the soil with carbonic
500 acid (CC_C). At CFEMS, the soil with the highest carbonate content, CC_C consumes about 60 g C
501 m^{-2} yr^{-1} of respired CO_2. In the soils of CFWMS, CC_C consumes respired CO_2 at the rate of 41 g
502 C m^{-2} yr^{-1}. These correspond to weathering rates of carbonate minerals due to carbonic acid of
503 5.0 and 3.5 mol carbonate m^{-2} yr^{-1} at CFEMS and CFWMS, consistent with the higher abundance
504 of carbonate minerals in CFEMS.
505 It should be noted that these calculations only account for reactions to the depth of the
506 deepest lysimeter at 108 cm and 190 cm at CFEMS and CFWMS, respectively. These deep
507 lysimeters are installed below the carbonate reaction fronts at the two sites and therefore

represent the interaction of porewaters with the carbonate minerals at CFEMS and CFWMS (Figs 2, 3; Table 1). Oversaturation of the lysimeter at 20 cm in the former soil likely is related to the occasional liming of the soils by past land managers.

3.6 Global Carbonate System Reactions

Maps of the carbonate-bearing soils (adapted from Batjes, 2016; and Thenkabail et al., 2016) represent lands in which carbonate minerals could affect soil CO_2 flux as discussed previously (Fig. 8). Soils that contain carbonate minerals and are neutral to basic represent about 98 million km^2 out of the global land area of 148 million km^2 (Fig. 8a). These soils favor inorganic carbon in the aqueous phase and could therefore lose dissolved C as a large fraction of soil respiration. Acidic agricultural soils that contain carbonate minerals represent about 7.4 million km^2 (Fig. 8b). Nitrification in these soils could support carbonate weathering (Eq. 2) and release CO_2 in the gas phase from the protons produced if pH were maintained low enough (Eq, 3).

520

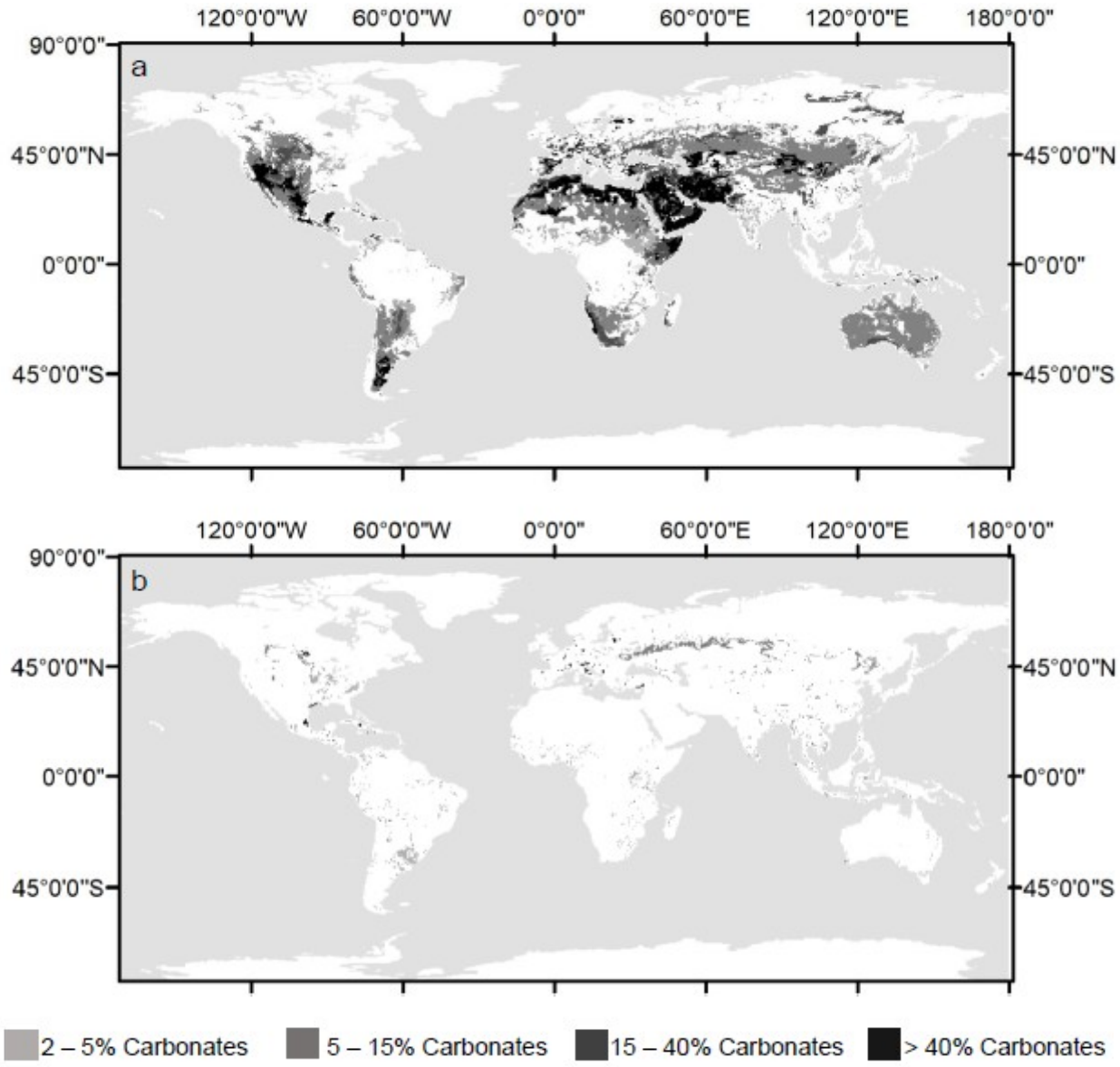

Fig 8: Soils with carbonates in the subsurface (30 – 100 cm) on a 0.5 degree raster grid classified by pH and land use. Darker cells indicate higher percent carbonates. The two panels represent different carbonate system processes that could affect soil CO_2 flux measurements and obscure interpretations of soil respiration rates. a) soils highlighted in this map represent neutral and basic soils underlain by carbonates. Conditions in these soils favor dissolution of respired CO_2 (and a lower CO_2 flux) and would result in underestimation of soil respiration rates b) soils highlighted in this panel represent acidic agricultural soils (pH < 5.5) with subsurface carbonates. Nitrification in these soils from application of fertilizers and manures may increase acidity and drive inorganic carbon into the gas phase. This would increase abiotic sources of CO_2 flux and lead to overestimates of soil respiration, if only surface CO_2 flux were measured.

4 Discussion

In support of hypothesis 1, our results show that hillslope position affects soil pCO_2, and this is largely due to differences in soil moisture conditions. The hillslope positions (CFEMS and CFWMS) with the highest soil moisture generated the highest pCO_2 over the 2018 growing season. Our results are consistent with other findings of soil moisture effects on respiration; higher soil moisture without prolonged saturation favors high root and microbial respiration rates and restricts diffusion of the CO_2 out of the soil profile (Brook et al., 1983; Hasenmueller et al., 2015; Pacific et al., 2010; Raich & Schlesinger, 1992). However, these soil moisture differences by hillslope position are not solely responsible for the variation in pCO_2 and pO_2 we observed at Cole Farm. The ARQ at the two calcareous soils was significantly less than 1, while the soil without carbonates indicated an ARQ of 1. Below we suggest that this difference in ARQ is likely due to the interaction of soil moisture with carbonate minerals at the midslopes (noting the lack of carbonates in the ridgetop soils). These interactions resulted in a greater proportion of respired CO_2 partitioned into the aqueous phase, supporting hypotheses 2 and 3. We also suggest that there is little evidence supporting hypothesis 4; i.e., carbonate weathering from nitrification acidity is not a source of gaseous CO_2 at our site.

4.1 Carbonate Mineralogy Affects Soil ARQ at Cole Farm Midslopes

The ARQ of ~1 at CFRT indicates that aerobic respiration and diffusion of CO_2 and O_2 are the dominant controls on soil pCO_2 at the ridgetop hillslope position where carbonates are largely lacking (Angert et al., 2015; Hodges et al., 2019). In contrast, at the midslopes, the ARQs are significantly less than 1, and these values indicate that aerobic respiration and diffusion are not the only controls on soil pCO_2. This points to the prevalence of a process that draws soil O_2 or CO_2 out of the gas phase. There is either less CO_2 in the gas phase than one would assume from the O_2 consumed in aerobic respiration, or there is less O_2 in the gas phase than one would

predict from the CO_2 produced via respiration. Here, we systematically examine these potential reactions and conclude that DIC export is the most likely cause for low ARQ in our midslope soils.

Nitrification by chemo-lithoautotrophs (Tsutsui et al., 2015) or metal oxidation (Hodges et al. 2019) can decrease O_2 to cause ARQ < 1, but our data enable us to rule out the possibility that these processes consume enough soil O_2 to shift ARQ at our sites. From our porewater NO_3^- concentrations, using the same estimation technique outlined in the methods section (Eq. 13), and based on the stoichiometry of nitrification (Eq. 6), we estimated that nitrification would remove about 4.5 g O_2 m^{-2} yr^{-1}. To shift the ARQ to a value comparable to our observations, nitrification rates would need to be two orders of magnitude greater, consuming about 450 g O_2 m^{-2} yr^{-1}. In forest soils of humid, temperate regions, oxidation of metals (mostly Fe) has also been pointed to as a potential mechanism of low ARQ (Angert et al., 2015; Hodges et al., 2019; Kim et al., 2017). However, total Fe concentrations at the three hillslope positions are similar (Table 1), and so one would expect an oxidation signature to be consistent at the three sites, rather than different. In fact, accounting for the differences in soil moisture, we would anticipate an oxidation signature (ARQ < 1) at CFRT and a reduction signature (ARQ > 1) at the midslopes; this is not what our measurements show.

If removal of gaseous O_2 is not driving low ARQ at our midslope sites, then a reaction that reduces soil pCO_2 must be at play, and we calculate that this "missing" CO_2 represents a substantial C flux in soils. The deviation of the midslope pCO_2-pO_2 regressions (Fig. 6) from slopes reflecting an ARQ of 1 represent C missing from the gaseous phase (Eq. 15; Sánchez-Cañete et al., 2018). At Cole Farm, we take the slope of -0.65, the regression slope at CFRT, to represent the aerobic baseline for the watershed (i.e. ARQ=1).

568 $$\frac{Actual\ Slope}{Aerobic\ Slope}=\frac{\frac{\Delta CO_{2Actual}}{\Delta O_{2Actual}}*\Delta O_{2Aerobic}}{\Delta CO_{2Aerobic}}=\frac{\Delta CO_{2Actual}}{\Delta CO_{2Aerobic}}=C_p(15)$$

569 Here we define ΔCO_2 as the change in pCO_2 for unit change of pO_2. If we assume that all
570 deviation in the regression slope is due to a change in pCO_2 and not pO_2, then ΔO_2, which is the
571 unit change of pO_2 for a change in pCO_2, of the actual slope and aerobic slopes cancel out.
572 Therefore, the ratio of the actual slope to the slope that represents aerobic respiration plus
573 diffusion gives us the fraction of CO_2 lost per unit change in O_2 for the measured soil compared
574 to the aerobic soil here called C_p (Eq. 15). Therefore, one minus C_p yields the fraction of CO_2 loss
575 missing from the measured soil, here C_m (Eq. 16).

576 $$1-C_p=C_m(16)$$

577 Once we calculate C_m we can then multiply it by the gaseous CO_2 flux for a similar site
578 that we know is dominantly controlled by aerobic respiration and diffusion, and this will allow us
579 to estimate the 'missing' gaseous CO_2 flux from Cole Farm. We know that about 1500 g C m^{-2}
580 yr^{-1} is the simulated root plus heterotrophic soil respiration rate of a nearby site where soil CO_2
581 flux is largely controlled by aerobic respiration and diffusion (Shi et al. 2018; Hodges et al.,
582 2019). Therefore, using equations 15 and 16, and then multiplying C_p by 1500 g C m^{-2}, we
583 estimate that 43% of the respired carbon or 645 g C m^{-2} yr^{-1} is missing from the gas phase flux at
584 CFEMS and 26% or 390 g C m^{-2} yr^{-1} is missing at CFWMS.

585 4.2 Where Is the "Missing" CO_2

586 At least three processes may account for the "missing" soil CO_2 that leads to ARQ < 1 at our
587 midslope sites: silicate weathering, carbonate weathering, or CO_2 dissolution in soil water.
588 Silicate minerals (here shown generically as $MSiO_3$) participate in acid-base weathering
589 reactions with DIC (Eq. 17), and if the DIC is removed in drainage, can represent a CO_2 sink.

590 $$MSiO_3 + 2\ CO_2 + H_2O \rightarrow M^{2+} + SiO_{2(aq)} + 2\ HCO_3^-$$ (17)

591 We can rule out this process because dissolution rates of the silicate minerals in shales of central
592 Pennsylvania are sufficiently slow that they have a negligible effect on soil pCO_2 at the temporal
593 resolution of our sampling (Hodges et al., 2019; Jin et al., 2014). Similarly, when we calculated
594 (see methods and results) CO_2-generated carbonate weathering reactions at the midslopes, we
595 observed that this would lower the gaseous CO_2 flux by 60 and 41 g C m^{-2} yr^{-1} at CFEMS and
596 CFWMS.

597 Thus, the last process that could account for the "missing" CO_2 from our midslope
598 profiles is CO_2 dissolution into porewaters and removal from the profile as DIC. Several lines of
599 evidence suggest that this is the most likely mechanism causing low ARQ in our midslope
600 profiles. The abundance of carbonate minerals, which buffer soil pH, along with high soil
601 moisture at these locations favor CO_2 dissolution and limit CO_2 diffusion out of the soil (Pacific
602 et al., 2010). However, high soil moisture alone cannot account for the observed differences in
603 ARQ. Saturated soil conditions without significant export would favor anaerobic respiration and
604 therefore an ARQ > 1, as wet soils limit O_2 diffusion and necessitate soil microbes to switch to
605 alternate terminal electron acceptors (Hodges et al., 2019). It is the interaction of high soil
606 moisture, efficient drainage, and mineralogy that enables high porewater pH and high
607 throughflux of water, which in turn increases the solubility of CO_2 in the porewater and loss of
608 DIC from the soil. The calculations in the results reflect this conclusion, as we found the greatest
609 deficit of respired CO_2 and highest carbonate weathering rate at CFEMS, the soil with the
610 highest carbonate mineral abundance.

611 These findings support hypothesis 2, as the carbonate mineralogy of the midslope soils
612 acts to facilitate the partitioning of respired CO_2 into DIC, some of which is transported deeper

and farther downslope or into deep groundwater. We are not the first to interpret a CO_2 dissolution signature from low ARQ. Olshansky et al. (2019) found that dissolution of soil CO_2 reduced soil CO_2 flux into the atmosphere by over half in a subhumid watershed underlain by metamorphic rocks. Additionally, Angert et al. (2015) reported ARQ values below 1 in calcareous soils in a Mediterranean climate that they attributed to CO_2 dissolution and carbonate weathering. However, while others have invoked CO_2 dissolution as the cause of ARQ < 1 (Angert et al., 2015; Olshansky et al., 2019; Sánchez-Cañete et al., 2018), we are the first to document such a pattern in a humid, temperate system. Our results indicate DIC export could be relevant in a range of ecosystems, as discussed in the section "*Extrapolating these Results Globally.*"

Our findings that a large proportion of respired CO_2 exports as DIC from the midslope soils of Cole Farm is comparable to other works. For example, a column experiment of dolomitic soils underlain by dolomite gravels found that respired C could account for 90 – 100% of the DIC that eluted from the column base. Like our findings at the midslopes, this study also found increased DIC export with both increased pCO_2 and soil moisture (Schindlbacher et al., 2019). Furthermore, Kindler et al. (2011) found that DIC export accounted for 25% of total C flux in a forest with a calcareous subsoil. This DIC export to groundwater serves as a temporary sink for respired C, perhaps for hundreds to thousands of years (Hamilton et al., 2007; Sanderman, 2012). However, this DIC likely degasses once it enters streams and rivers, changing the time and place of the eventual CO_2 efflux (Butman & Raymond, 2011). Our results underline that partitioning of respired C to the aqueous phase represents an important C flux that should be accounted for when measuring soil C fluxes and accounting for watershed C balance.

635 4.3 Nitric Acid Has a Negligible Effect on ARQ and Partitioning of CO_2

636 We also explored the role of nitric acid-promoted carbonate weathering in driving carbonate-
637 derived CO_2 into the gaseous phase. While our calculations show that NO_3^- in the porewaters is
638 associated with carbonate dissolution, both the ARQ at the midslope soils and our calculations
639 show that the contribution of these reactions to gaseous CO_2 flux is negligible to non-existent.
640 The soil atmosphere in the carbonate-bearing soils at Cole Farm show a lack, not a surplus, of
641 gaseous CO_2 relative to O_2. Our results refute hypothesis 4 since our results did not indicate
642 gaseous CO_2 release from nitrification-associated carbonate weathering.

643 Our findings are comparable to those found by others working in agricultural systems
644 underlain by carbonate-bearing rocks. For example, Perrin et al. (2008) found that N fertilization
645 resulted in a higher proportion of stream cations balanced by NO_3^- than HCO_3^-. They estimated
646 that this NO_3^- replaced 7-17% of the HCO_3^- in rivers, comparable to our estimates from lysimeter
647 samples at CFEMS and CFWMS. A follow-up study to Perrin et al. indicated that the acidity
648 from nitrification did not lower soil pH sufficiently in carbonate systems to drive carbonate-
649 derived CO_2 into the gas phase (Gandois et al., 2011). Likewise, in laboratory column
650 experiments, Song et al. (2017) found that all ammoniacal fertilizers increase carbonate
651 weathering rates compared to organic N or urea, but that they do not sufficiently lower pH to
652 drive CO_2 into the gaseous phase.

653 However, some workers have estimated large abiotic CO_2 fluxes associated with
654 nitrification in agricultural systems (Zamanian et al., 2018, 2021). The key difference between
655 our results and those of Zamanian et al. (2018) are that Zamanian et al. (2018) assume that all
656 nitrate-promoted weathering reactions result in CO_2 in the gaseous phase. In reality, soil
657 moisture, pH, temperature, and distribution of carbonates in the soil profile determine whether a
658 gaseous CO_2 flux is a reasonable outcome from the weathering of carbonates by nitrification

associated acidity. More specifically, this gaseous CO_2 flux is only reasonable if there is a high rate of nitrification and a small amount of carbonate minerals present such that the acid input outstrips the capacity of carbonate minerals to buffer solution pH. Indeed, Hamilton et al. (2007) found that reaction of carbonic acid derived from root and microbial respiration with agricultural lime far outpaces the generation of CO_2 caused by nitric acid reacting with carbonate minerals. West & McBride (2005) estimated that about 40% of C in agricultural lime eventually degasses from soils or riverine systems. Contrary to the hypothesis of Zamanian et al. (2018), the results of Hamilton et al. (2007) and West & McBride (2005) together suggest that agricultural lime has either a net-zero impact on CO_2 efflux or acts as a small C sink. Thus, our results and the work of others call for a nuanced approach when estimating effects of N fertilization on carbonate weathering and potential gaseous CO_2 emissions from nitrification-associated acidity reacting with carbonate-bearing minerals.

4.4 Extrapolating These Results Globally

Clearly DIC loss in the aqueous phase represents an important component of soil C flux in many systems, and this partitioning between gaseous and aqueous phases is not yet appreciated in short-timescale C cycle modeling. In this section we explore the potential global significance of the reactions we have detailed in this discussion with a mapping exercise.

Soil inorganic C (SIC) comprises over one third of the global soil carbon pool and it may be particularly sensitive to changes in land use and climate (Ahmad et al., 2015; Bargrizan et al., 2020; Zamanian et al., 2016). Reactions of SIC in the soil system have disparate effects on soil CO_2 flux, and those effects are difficult to parse by magnitude and scale. Therefore, we mapped the global distribution of carbonate-bearing soils likely affected by the reactions we explored at Cole Farm. First, we mapped soils in which CO_2 dissolution into soil water that leaves the soil

682 acts as a sink for gaseous CO_2, lowering soil CO_2 fluxes (Fig. 8a). Second, based on the slow rate
683 of nitrification-induced weathering at Cole Farm, we modified the mapped soils in Zamanian et
684 al. (2018) to sites we think may actually have an abiotic soil CO_2 flux due to nitric acid from
685 fertilizers that dissolve carbonate minerals and decrease the soil pH to favor an efflux of CO_2
686 into the gaseous phase (Fig. 8b).

687 At about 98 million km^2, the carbonate-bearing soils that we hypothesize will lose
688 respired C through CO_2 dissolution in porewaters and weathering reactions represent far greater
689 land area than the 7.4 km^2 of agricultural soils with N fertilization and acidic pH. Based on our
690 work and others, dissolution of respired CO_2 in carbonate-bearing soils with neutral and basic pH
691 can reduce soil CO_2 flux by over one half (Olshansky et al., 2019; Sánchez-Cañete et al., 2018);
692 DIC export from many of these carbonate systems may represent a large C export from soils
693 during the growing season (Kindler et al., 2011), or after extreme precipitation events (T. Liu et
694 al., 2018b). In fact, some soils show decreasing pCO_2 with depth at the deepest depths, consistent
695 with drawdown by drainage of DIC (Brantley et al., 2014; Stinchcomb et al., 2018). This loss of
696 DIC derived from mineral weathering is a sink for respired C (Bargrizan et al., 2020).

697 While dissolution of respired CO_2 may be predominant in these soils, much of this land
698 area is desert in which soil respiration and moisture are low. Therefore, the effect of this desert
699 land on the global carbon cycle is minor. However, as rainfall or irrigation increases soil
700 moisture, more CO_2 dissolves in porewaters to weather carbonate minerals (Kim et al., 2020;
701 Raza et al., 2020). Even in the desert soils in dry lands, eddy covariance flux studies have
702 documented anomalous CO_2 consumption. For example, Wolfahrt et al. (2008) found large
703 annual CO_2 uptake rates in the Mojave Desert. After review, most attribute such C uptake in
704 cases like those described by Wolfahrt et al. (2008) to carbonate mineral dissolution (Cueva et

al., 2019; Kowalski et al., 2008; Rey, 2015; Serrano-Ortiz et al., 2010). Evidence of the significance of dissolved inorganic carbon fluxes in these soils from across a range of ecosystems underlines that DIC and carbonate system reactions must be accounted for when constructing watershed carbon budgets.

On the other hand, acidic agricultural soils that also contain carbonates cover 7.4 million km^2, or about 4.6% of the terrestrial surface area of the earth. While these soils are scattered, there are large pockets in centers of agricultural production within Canada, the United States, Uruguay, Argentina, Western Europe, and Russia (Fig. 8b). It is in these soils that we may expect to observe an increase in soil CO_2 flux from nitrification-derived acidity enhancing carbonate weathering. This estimated land area is much less than previous estimates of nitrification-affected carbonate soils (Zamanian et al., 2018) because we only mapped soils with a pH < 5.5 that would favor CO_2 in the gas phase. For other neutral and basic soils where nitric acid weathering occurs, it is likely that the abiotically released CO_2 remains dissolved in soil water. Even in the warm, acidic soils in which gaseous CO_2 is most favored, and at the highest range of estimated CO_2 production from proton-promoted carbonate dissolution in Zamanian et al., (2018), the CO_2 flux would only be 5 g C m^{-2} yr^{-1}. While potentially important in certain cases, it is likely within error of most watershed C budget studies.

However, our maps do not provide a complete picture of the potential soils affected by the two scenarios outlined above. The resolution of figure 8, and even the USDA soil survey, do not allow prediction of the extent of variability in soil mineralogy as that which we observed at Cole Farm. This highlights the importance of such mineralogical and elemental analyses of soils when conducting ecosystem C cycle research.

727 Our soil gas and porewater chemistry indicate that the measured differences in elemental
728 composition influence the C cycle and weathering reactions in our watershed and impart strong
729 spatial heterogeneity on CO_2 partitioning between gas and aqueous phase. High soil moisture and
730 neutral pH buffered by carbonate minerals at the midslopes drove CO_2 dissolution and imparted
731 an ARQ lower at the midslopes than the ridgetop. Differences in soil mineralogy controlled
732 further CO_2 dissolution through carbonate weathering reactions. While accounting for some of
733 the carbonate weathering, nitrification did not have a measurable effect on the soil CO_2 at Cole
734 Farm. We conclude that assessing soil and lithologic properties is key when measuring the soil C
735 cycle in a watershed. Furthermore, our results provide strong evidence that DIC can be a
736 significant component of the C cycle in humid, temperate watersheds. In our case, surface soil
737 CO_2 efflux would greatly underestimate soil respiration, confounding efforts to construct or
738 simulate the soil C cycle using traditional surface efflux measurements. Globally, these
739 carbonate system reactions have the capacity to alter the balance of C pools and fluxes in many
740 ecosystems, especially with shifting land use.

741

742 **Acknowledgments, Samples, and Data**

743 Financial Support was provided by National Science Foundation Grant EAR – 1331726
744 to SLB for SSHCZO and NIFA Predoctoral Fellowship 2020-67034-31716 to CH. This research
745 was conducted on a farm in Shaver's Creek watershed at the intersection of RT 305 and
746 Winchester Road and we acknowledge the support of the owner, H. Cole. Thanks to Benjamin
747 Dillner and Brosi Bradley for field assistance and Xin Gu, Alison Richards, and Perri Silverhart
748 for rock sampling and interpretation of regional geology and mineralogy. Porewaters and rocks
749 were analyzed at the Laboratory for Isotopes and Metals in the Environment at Pennsylvania

State University. Soil moisture time series, soil profile descriptions, and soil profile geochemistry are available at czo.psu.edu. Soil porewater chemistry and soil pCO_2 and pO_2 will be published as coordinated datasets in Pangaea (pangaea.de).

References

Amundson, R. (2001). The Carbon Budget in Soils. Annual Review of Earth and Planetary Sciences, 29(1), 535–562. https://doi.org/10.1146/annurev.earth.29.1.535

Ahmad, W., Singh, B., Dalal, R. C., & Dijkstra, F. A. (2015). Carbon dynamics from carbonate dissolution in Australian agricultural soils. *Soil Research*, *53*(2), 144–153. https://doi.org/10.1071/sr14060

Angert, A., Yakir, D., Rodeghiero, M., Preisler, Y., Davidson, E. A., & Weiner, T. (2015). Using O2 to study the relationships between soil CO2 efflux and soil respiration. *Biogeosciences*, *12*(7), 2089–2099. https://doi.org/10.5194/bg-12-2089-2015

Bargrizan, S., Smernik, R. J., & Mosley, L. M. (2020). Constraining the carbonate system in soils via testing the internal consistency of pH, pCO2 and alkalinity measurements. *Geochemical Transactions*, *21*(1), 4. https://doi.org/10.1186/s12932-020-00069-5

Batjes, N. (2016). Harmonized soil property values for broad-scale modelling (WISE30sec) with estimates of global soil carbon stocks *Geoderma* 269, 61-68. https://dx.doi.org/10.1016/j.geoderma.2016.01.034

Brantley, S.L., Lebedeva, M., & Bazilevskaya, E. (2014). *Treatise on Geochemistry (Second Edition)*. 327–352. https://doi.org/10.1016/B978-0-08-095975-7.01317-6

Brantley, S.L., Holleran, M. E., Jin, L., & Bazilevskaya, E. (2013). Probing deep weathering in the Shale Hills Critical Zone Observatory, Pennsylvania (USA): The hypothesis of nested chemical reaction fronts in the subsurface. *Earth Surface Processes and Landforms*, *38*(11), 1280–1298. https://doi.org/10.1002/esp.3415

Butman, D., & Raymond, P. A. (2011). Significant efflux of carbon dioxide from streams and rivers in the United States. *Nature Geoscience*, *4*(12), 839. https://doi.org/10.1038/ngeo1294

Cerling, T. E. (1984). The stable isotopic composition of modern soil carbonate and its relationship to climate. *Earth and Planetary Science Letters*, *71*(2), 229–240. https://doi.org/10.1016/0012-821x(84)90089-x

Chadwick, O. A., Kelly, E. F., Merritts, D. M., & Amundson, R. G. (1994). Carbon dioxide consumption during soil development. *Biogeochemistry*, *24*(3), 115–127. https://doi.org/10.1007/bf00003268

Cueva, A., Volkmann, T. H. M., Haren, J. van, Troch, P. A., & Meredith, L. K. (2019). Reconciling Negative Soil CO_2 Fluxes: Insights from a Large-Scale Experimental Hillslope. *Soil Systems*, *3*(1), 10. https://doi.org/10.3390/soilsystems3010010

Doane, T. A., & Horwáth, W. R. (2003). Spectrophotometric determination of nitrate with a single reagent. Analytical Letters, 36(12), 2713–2722. https://doi.org/10.1081/AL-120024647

Gandois, L., Perrin, A.-S., & Probst, A. (2011). Impact of nitrogenous fertiliser-induced proton release on cultivated soils with contrasting carbonate contents: A column experiment. *Geochimica et Cosmochimica Acta*, *75*(5), 1185–1198. https://doi.org/10.1016/j.gca.2010.11.025

Gu, X., Mavko, G., Ma, L., Oakley, D., Accardo, N., Carr, B. J., et al. (2020). Seismic refraction tracks porosity generation and possible CO2 production at depth under a headwater catchment. *Proceedings of the National Academy of Sciences*, *117*(32), 18991–18997. https://doi.org/10.1073/pnas.2003451117

Hamerlynck, E. P., Scott, R. L., Sánchez−Cañete, E. P., & Barron−Gafford, G. A. (2013). Nocturnal soil CO2 uptake and its relationship to subsurface soil and ecosystem carbon fluxes in a Chihuahuan Desert shrubland. *Journal of Geophysical Research: Biogeosciences*, *118*(4), 1593–1603. https://doi.org/10.1002/2013jg002495

Hamilton, S. K., Kurzman, A. L., Arango, C., Jin, L., & Robertson, G. P. (2007). Evidence for carbon sequestration by agricultural liming. *Global Biogeochemical Cycles*, *21*(2). https://doi.org/10.1029/2006gb002738

Hasenmueller, E., Jin, L., Stinchcomb, G., Lin, H., Brantley, S., Kaye, J. (2015). Topographic controls on the depth distribution of soil CO_2 in a small temperate watershed. *Applied Geochemistry*. 63, 58-69. https://dx.doi.org/10.1016/j.apgeochem.2015.07.005

Hodges, C., Kim, H., Brantley, S. L., & Kaye, J. (2019). Soil CO_2 and O_2 Concentrations Illuminate the Relative Importance of Weathering and Respiration to Seasonal Soil Gas Fluctuations. *Soil Science Society of America Journal*. https://doi.org/10.2136/sssaj2019.02.0049

Jin, L., Ogrinc, N., Yesavage, T., Hasenmueller, E. A., Ma, L., Sullivan, P. L., et al. (2014). The CO_2 consumption potential during gray shale weathering: Insights from the evolution of carbon isotopes in the Susquehanna Shale Hills critical zone observatory. *Geochimica et Cosmochimica Acta*, 142, 260–280. https://doi.org/10.1016/j.gca.2014.07.006

Kim, H., Stinchcomb, G., & Brantley, S. L. (2017). Feedbacks among O2 and CO2 in deep soil gas, oxidation of ferrous minerals, and fractures: A hypothesis for steady-state regolith thickness. *Earth and Planetary Science Letters*, *460*, 29–40. https://doi.org/10.1016/j.epsl.2016.12.003

Kim, J. H., Jobbágy, E. G., Richter, D. D., Trumbore, S. E. & Jackson, R. B. (2020). Agricultural acceleration of soil carbonate weathering. *Global Change Biology.* 26, 5988–6002. 10.1111/gcb.15207

Kindler, R., Siemens, J., Kaiser, K., Walmsley, D. C., Berhoffer, C., Buchmann, N., Cellar, P., Eugster, W., Gliexner, G., Grunwald, T., Heim, A., Ibrom, A., Jones, S. K., Jones, M., Klumpp, K., Kutsch, W., Larsen, K. S., Lehuger, S., Loubett, B., … Kaupenjohann, M. (2011). Dissolved carbon leaching from soil is a crucial component of the net ecosystem carbon balance. *Global Change Biology*, *17*(2), 1167–1185. https://doi.org/10.1111/j.1365-2486.2010.02282.x

Kowalski, A. S., Serrano-Ortiz, P., Janssens, I. A., Sánchez-Moral, S., Cuezva, S., Domingo, F., Were, A., & Alados-Arboledas, L. (2008). Can flux tower research neglect geochemical CO_2 exchange? *Agricultural and Forest Meteorology*, *148*(6–7), 1045–1054. https://doi.org/10.1016/j.agrformet.2008.02.004

Li, L., Bao, C., Sullivan, P. L., Brantley, S., Shi, Y., & Duffy, C. (2017). Understanding watershed hydrogeochemistry: 2. Synchronized hydrological and geochemical processes drive

stream chemostatic behavior. *Water Resources Research*, *53*(3), 2346–2367. https://doi.org/10.1002/2016wr018935

Li, L., DiBiase, R. A., Vecchio, J. D., Marcon, V., Hoagland, B., Xiao, D., Wayman, C., Tang, Q., He, Y., Silverhart, P., Szink, I., Forsythe, B., Williams, J. Z., Shapich, D., Mount, G. J., Kaye, J., Guo, L., Lin, H., Eissenstat, D., … Brantley, S. L. (2018). The Effect of Lithology and Agriculture at the Susquehanna Shale Hills Critical Zone Observatory. *Vadose Zone Journal*, *17*(1), 0. https://doi.org/10.2136/vzj2018.03.0063

Liu, J., Fa, K., Zhang, Y., Wu, B., Qin, S., & Jia, X. (2015). Abiotic CO 2 uptake from the atmosphere by semiarid desert soil and its partitioning into soil phases. *Geophysical Research Letters*, *42*(14), 5779–5785. https://doi.org/10.1002/2015gl064689

Liu, T., Wang, L., Feng, X., Zhang, J., Ma, T., Wang, X., & Liu, Z. (2018a). Comparing soil carbon loss through respiration and leaching under extreme precipitation events in arid and semiarid grasslands. *Biogeosciences*, *15*(5), 1627–1641. https://doi.org/10.5194/bg-15-1627-2018

Liu, T., Wang, L., Feng, X., Zhang, J., Ma, T., Wang, X., & Liu, Z. (2018b). Comparing soil carbon loss through respiration and leaching under extreme precipitation events in arid and semiarid grasslands. *Biogeosciences*, *15*(5), 1627–1641. https://doi.org/10.5194/bg-15-1627-2018

Lloyd, J., & Taylor, J. (1994). On the Temperature Dependence of Soil Respiration. *Functional Ecology, 8*(3), 315-323. doi:10.2307/2389824

Mikhailova, E. A., & Post, C. J. (2006). Effects of Land Use on Soil Inorganic Carbon Stocks in the Russian Chernozem. Journal of Environmental Quality, 35(4), 1384–1388. https://doi.org/10.2134/jeq2005.0151

NADP (National Atmospheric Deposition Program). (2018). Leading Ridge (PA42) site, annual precipitation-weighted means [Data set]. Retrieved from http://nadp.sws.uiuc.edu/data/NTN/

Nychka, D., R. Furrer, J. Paige, and S. Sain. 2017. Fields: Tools for spatial data. University Corporation for Atmospheric Research, Boulder, CO. doi:10.5065/D6W957CT

Oleson, K. W., Lawrence, D. M., Gordon, B., Flanner, M. G., Kluzek, E., Peter, J., ... & Heald, C. L. (2010). Technical description of version 4.0 of the Community Land Model (CLM).

Olshansky, Y., Knowles, J. F., Barron‐Gafford, G. A., Rasmussen, C., Abramson, N., & Chorover, J. (2019). Soil Fluid Biogeochemical Response to Climatic Events. *Journal of Geophysical Research: Biogeosciences*. https://doi.org/10.1029/2019jg005216

Pacific, V. J., McGlynn, B. L., Riveros-Iregui, D. A., Welsch, D. L., & Epstein, H. E. (2010). Landscape structure, groundwater dynamics, and soil water content influence soil respiration across riparian-hillslope transitions in the Tenderfoot Creek Experimental Forest, Montana. *Hydrological Processes*, *25*(5), 811–827. https://doi.org/10.1002/hyp.7870

Perrin, A.-S., Probst, A., & Probst, J.-L. (2008). Impact of nitrogenous fertilizers on carbonate dissolution in small agricultural catchments: Implications for weathering CO2 uptake at regional and global scales. *Geochimica et Cosmochimica Acta*, *72*(13), 3105–3123. https://doi.org/10.1016/j.gca.2008.04.011

R Core Team. 2018. R: A language and environment for statistical computing. R Foundation for Statistical Computing, Vienna, Austria.

Raich, J. W., & Schlesinger, W. H. (1992). The global carbon dioxide flux in soil respiration and its relationship to vegetation and climate. *Tellus B: Chemical and Physical Meteorology*, *44*(2), 81–99. https://doi.org/10.3402/tellusb.v44i2.15428

Raza S., N. Miao, P. Wang, X. Ju, Z. Chen, J. Zhou, Y. Kuzyakov. (2020). Dramatic loss of inorganic carbon by nitrogen−induced soil acidification in Chinese croplands. *Global Change Biology*. 26, 3738–3751. 10.1111/gcb.15101

Rey, A. (2015). Mind the gap: Non−biological processes contributing to soil CO2 efflux. *Global Change Biology*, *21*(5), 1752–1761. https://doi.org/10.1111/gcb.12821

Sánchez-Cañete, E. P., Barron-Gafford, G. A., & Chorover, J. (2018). A considerable fraction of soil-respired CO2 is not emitted directly to the atmosphere. *Scientific Reports*, *8*(1), 13518. https://doi.org/10.1038/s41598-018-29803-x

Sanderman, J. (2012). Can management induced changes in the carbonate system drive soil carbon sequestration? A review with particular focus on Australia. *Agriculture, Ecosystems & Environment*, *155*, 70–77. https://doi.org/10.1016/j.agee.2012.04.015

Schindlbacher, A., Beck, K., Holzheu, S., & Borken, W. (2019). Inorganic Carbon Leaching From a Warmed and Irrigated Carbonate Forest Soil. *Frontiers in Forests and Global Change*, *2*, 40. https://doi.org/10.3389/ffgc.2019.00040

Serrano-Ortiz, P., Roland, M., Sanchez-Moral, S., Janssens, I. A., Domingo, F., Goddéris, Y., & Kowalski, A. S. (2010). Hidden, abiotic CO2 flows and gaseous reservoirs in the terrestrial carbon cycle: Review and perspectives. *Agricultural and Forest Meteorology*, *150*(3), 321–329. https://doi.org/10.1016/j.agrformet.2010.01.002

Shi, Y., Eissenstat, D. M., He, Y., & Davis, K. J. (2018). Using a spatially-distributed hydrologic biogeochemistry model with a nitrogen transport module to study the spatial variation of carbon processes in a Critical Zone Observatory. *Ecological Modelling*, *380*, 8–21. https://doi.org/10.1016/j.ecolmodel.2018.04.007

Silverhart, P. (2019). *Land use versus climate controls on hillslope erosion at a farmed headwater catchment in central Pennsylvania* (Unpublished Master's Thesis). Pennsylvania State University, University Park, PA.

Sims, G. K., Ellsworth, T. R., & Mulvaney, R. L. (1995). Microscale determination of inorganic nitrogen in water and soil extracts. Communications in Soil Science and Plant Analysis, 26(1–2), 303–316. https://doi.org/10.1080/00103629509369298

Stumm, W., & Morgan, J. J. (1996). *Aquatic Chemistry*. 477.

Thenkabail, P., Knox, J., Ozdogan, M., Gumma, M., Congalton, R., Wu, Z., Milesi, C., Finkral, A., Marshall, M., Mariotto, I., You, S., Giri, C., Nagler, P. (2016). NASA Making Earth System Data Records for Use in Research Environments (MEaSUREs) Global Food Security Support Analysis Data (GFSAD) Crop Dominance 2010 Global 1 km V001 [Data set]. NASA EOSDIS Land Processes DAAC. Accessed 2020-01-23 from https://doi.org/10.5067/MEaSUREs/GFSAD/GFSAD1KCD.001

Thornton, P. E., Law, B. E., Gholz, H. L., Clark, K. L., Falge, E., Ellsworth, D. S., Goldstein, A. H., Monson, R. K., Hollinger, D., Falk, M., Chen, J., & Sparks, J. P. (2002). Modeling and measuring the effects of disturbance history and climate on carbon and water budgets in evergreen needleleaf forests. *Agricultural and Forest Meteorology*, *113*(1), 185–222.

Tsutsui, H., Fujiwara, T., Inoue, D., Ito, R., Matsukawa, K., & Funamizu, N. (2015). Relationship between respiratory quotient, nitrification, and nitrous oxide emissions in a forced aerated composting process. *Waste Management*, *42*, 10–16. https://doi.org/10.1016/j.wasman.2015.02.038

West, T. O., & McBride, A. C. (2005). The contribution of agricultural lime to carbon dioxide emissions in the United States: dissolution, transport, and net emissions. Agriculture, Ecosystems & Environment, 108(2), 145–154. https://doi.org/10.1016/j.agee.2005.01.002

Wu, L., Wood, Y., Jiang, P., Li, L., Pan, G., Lu, J., et al. (2008). Carbon Sequestration and Dynamics of Two Irrigated Agricultural Soils in California. Soil Science Society of America Journal, 72(3), 808–814. https://doi.org/10.2136/sssaj2007.0074

Zamanian, K., Pustovoytov, K., & Kuzyakov, Y. (2016). Pedogenic carbonates: Forms and formation processes. *Earth-Science Reviews*, *157*, 1–17. https://doi.org/10.1016/j.earscirev.2016.03.003

Zamanian, K., Zarebanadkouki, M., & Kuzyakov, Y. (2018). Nitrogen fertilization raises CO_2 efflux from inorganic carbon: A global assessment. *Global Change Biology*, *24*(7), 2810–2817. https://doi.org/10.1111/gcb.14148

Zamanian, K., Zhou, J., & Kuzyakov, Y. (2021). Soil carbonates: The unaccounted, irrecoverable carbon source. Geoderma, 384, 114817. https://doi.org/10.1016/j.geoderma.2020.114817